RSC Advances

PAPER

View Article Online
View Journal | View Issue

Cite this: *RSC Adv.*, 2017, **7**, 5610

Uncovering the metastable γ-Ag_2WO_4 phase: a joint experimental and theoretical study†

Roman Alvarez Roca,*[a] Pablo S. Lemos,[a] Lourdes Gracia,[b] Juan Andrés[b] and Elson Longo[a]

Received 3rd October 2016
Accepted 8th November 2016

DOI: 10.1039/c6ra24692c

www.rsc.org/advances

The synthesis of metastable solid phases is a pivotal starting point for innovative materials research. Here, we report the synthesis by means of a precipitation method of the metastable cubic γ-Ag_2WO_4 phase under ambient conditions. Different experimental techniques such as X-ray diffraction (XRD) with Rietveld refinement, field emission scanning electron microscopy (FE-SEM), micro-Raman/ultraviolet-visible (UV-vis) diffuse reflectance, photoluminescence spectroscopies, and differential scanning calorimetry (DSC) were employed. To complement the experimental data, the geometry, morphology, vibrational and electronic structure of γ-Ag_2WO_4 were characterized and evaluated using first-principles quantum mechanical calculations at the density functional theory (DFT) level. A theoretical model based on the Wulff construction was introduced to explain the possible crystal morphologies of the faceted crystals, which were obtained by tuning the surface chemistry of the crystals, and are related to their relative stability. Both the experimental and theoretical data revealed the presence of (100), (110), and (111) facets with low surface energies in the γ-Ag_2WO_4 crystals. When the surface energy value of the (111) surface was lowered, the experimental morphologies of the as-synthesized samples were similar to the theoretically obtained shapes. From the analysis of the experimental and calculated Raman spectra, PL emissions, and the density of states, we can assume that γ-Ag_2WO_4 is primarily formed by both distorted clusters: [WO_4] tetrahedra and, distorted in a lesser extent, [AgO_6] octahedra.

1. Introduction

Polymorphism is the ability of a given material to exist in more than one form, that is, to have different crystal structures and properties, while maintaining the same chemical composition. Polymorphism is a key property that enables researchers to investigate different structures depending on external conditions, such as temperature, pressure, type of field (electric, magnetic, *etc.*), synthetic procedure, and mode and duration of the material processing, *i.e.*, the enhancement of a particular phase modification, out of all possible polymorphic phases, depends on the thermodynamic and kinetic factors. Research on the synthesis of metastable material phases has been fueled by studies where it has been found that these phases exhibit unexplored physical and chemical properties that are distinct from the properties of their thermodynamically stable counterparts.[1–5] However, these studies have been incomplete due to the propensity of the metastable phases to transform into more stable phases. In addition, the challenge to develop facile methods for the synthesis of metastable materials remains.[6,7] Thus, it would be highly desirable to investigate metastable material phases in a manner similar to that adopted for the thermodynamically stable ones, so as to put both on a comparable footing.

Silver tungstate (Ag_2WO_4)-based materials constitute a particularly intensively researched family of inorganic compounds because of their particular crystal and electronic structures.[8–12] In response to their extensive range of innovative properties and practical applications, a plethora of experimental works have been published on the synthesis and properties of Ag_2WO_4-based materials,[13–26] and on their applications in photocatalysis,[17,19,20,25] catalysis,[14,18] photoluminescence,[9,13,15] sensors,[22] and as antibacterial agents.[21,23,26] Ag_2WO_4 exhibits stunningly complex polymorphism,[27] and its understanding has evoked recent interest due to both fundamental scientific and technological aspects. Apart from the orthorhombic and thermodynamically stable α-Ag_2WO_4 phase, β- and γ-phases have also been identified with hexagonal and cubic structures, respectively.[27] In addition, it has been well established that these β- and γ-phases are metastable phases that can be transformed into the α-phase when heated.

To date, different synthesis methods have been reported in the literature to obtain Ag_2WO_4 metastable phases.[27–33] In particular, β-Ag_2WO_4 was successfully prepared by a precipitation

[a]*CDMF-UFSCar-Universidade Federal de São Carlos, P.O. Box 676, CEP, 13565-905 São Carlos, SP, Brazil*

[b]*Department of Analytical and Physical Chemistry, University Jaume I (UJI), Castelló 12071, Spain. E-mail: andres@qfa.uji.es*

† Electronic supplementary information (ESI) available. See DOI: 10.1039/c6ra24692c

method using a surfactant-assisted route in the presence of polymethacrylic acid (PMAA),[28] acrylamide (AM),[26] or polyvinylpyrrolidone (PVP).[29] The transformation from the metastable β-phase to the thermodynamically stable α-phase was inhibited by the surfactant. Without the addition of any surfactants, other conditions (such as temperature and pH) can serve as inhibitors to prevent this phase transformation. For example, a metastable β-Ag_2WO_4 phase, which coexisted with a weak amount of α-phase, was obtained using a co-precipitation method at pH 4;[31] in addition, the synthesis of pure β-Ag_2WO_4 at low temperatures has also been reported.[30] Recently, our research group reported the synthesis of β-Ag_2WO_4 microcrystals by simple[34] and drop-wise precipitation[35] methods. Moreover, Gupta *et al.* presented a new strategy for synthesizing hexagonal metastable β-Ag_2WO_4 at room temperature through the use of aliovalent Eu^{3+} dopants (to induced the orthorhombic (α-Ag_2WO_4) to hexagonal (β-Ag_2WO_4) phase transition) along with the co-precipitation method.[36] Less is known about the γ-Ag_2WO_4 phase due to its scarcity and complex synthesis, and practically no attempt has been reported regarding the formation of a pure,-metastable γ-Ag_2WO_4.[27,32,33] Thus, the transfer of all the preceding experiments to the corresponding cubic phase is most rewarding with respect to elucidating the common properties and differences between the α- and β-Ag_2WO_4 modifications.

The simultaneous use of theoretical calculations alongside experiments has been a significant aid for the interpretation and assignment of complex spectra. This combination has previously been applied to the investigation of complex materials such as β-Ag_2WO_4,[35] Ag_2CrO_4,[37] and $Ag_4V_2O_7$ (ref. 38) crystals. To the best of our knowledge, combination of theoretical and experimental studies on the structure of γ-Ag_2WO_4 crystals is inexistent. This encouraged us to investigate the geometry, cluster coordination, and electronic structure of γ-Ag_2WO_4 crystals.

Herein, for the first time, the facile synthesis and characterization of the metastable cubic γ-Ag_2WO_4 phase is reported. Different experimental techniques such as X-ray diffraction (XRD) with Rietveld refinement, field emission scanning electron microscopy (FE-SEM), micro-Raman/ultraviolet-visible (UV-vis) diffuse reflectance, photoluminescence (PL) spectroscopies, and differential scanning calorimetry have been employed. In addition, the geometry, electronic structure, morphology, and optical properties of the γ-Ag_2WO_4 phase were investigated with first-principles quantum mechanical calculations at the density functional theory (DFT) level, and the theoretical results were compared with the experimental data. The calculations helped us to interpret and understand the physical mechanisms that drive the experimental results. The remainder of this paper is organized as follows: Section 2 describes the experimental procedure and computational details; Section 3 contains the results and discussion; and Section 4 provides a summary of this study and the concluding remarks.

2. Experimental

2.1 Material synthesis

High-purity silver nitrate ($AgNO_3$; 99.8% purity, Sigma-Aldrich) and sodium tungstate ($Na_2WO_4 \cdot 2H_2O$; 99.0% purity, Sigma-Aldrich) were obtained from commercial sources and used as received. The γ-Ag_2WO_4 phase was obtained by simultaneous addition of 1.13 g (6.66 mmol) of $AgNO_3$ and 1.10 g (3.33 mmol) of $Na_2WO_4 \cdot 2H_2O$ in 20 mL of deionized water. The reaction was performed under low temperature conditions (0–5 °C) and under continuous stirring. In order to have a better understanding of the process of formation of the γ-Ag_2WO_4 particles, the reaction progress was checked in two moments: one portion was extracted of the reaction after 10 min and then the precipitate was collected; and the second portion was allowed to react for another 10 min, for a total 20 min reaction time. Subsequently, the two portions were washed several times with acetone and dried at 50 °C.

2.2 Characterization

In order to determine the crystal phase, X-ray diffraction (XRD) measurements were carried out using a D/max-2000/PC X-ray powder diffractometer (Rigaku) with Cu Kα radiation at a scanning speed of 2° min^{-1}. The XRD accelerating voltage and emission current were 40 kV and 30 mA, respectively. The microstructure and surface characteristics were investigated using an FE-SEM Inspect F50 (FEI Company, Hillsboro, OR) apparatus operated at 10 kV. High-resolution Raman spectra were recorded with a He–Ne laser at 632.81 nm (model CCD DU420AOE325) operating at 25–1000 cm^{-1}, keeping its maximum output power at 6 mW. The transformation of the material during its heat treatment was studied by differential scanning calorimetry (DSC) using an STA 409/429 Netzsch instrument at a rate of 10 °C min^{-1} from 25 to 700 °C. UV-vis diffuse reflectance spectra measurements were carried out using a Varian spectrophotometer (model Cary 5G) at the 100–800 nm wavelength analysis range. Photoluminescence emission spectra were recorded on a Monospec 27 monochromator (Thermal Jarrel Ash) coupled to an R446 (Hamamatsu Photonics) photomultiplier, and a krypton-ion laser (Coherent Innova 90K; $\lambda = 350$ nm), over a wavelength range of 350–850 nm.

2.3 Computational details

Calculations on the periodic γ-Ag_2WO_4 structure were performed with the CRYSTAL14 software package.[39] For the calculations, tungsten was described by a large-core ECP, derived by Hay and Wadt, and modified by Cora *et al.*,[40] while the silver and oxygen centers were described using HAYWSC-311d31G and O (6-31d1G) basis sets, respectively, which were taken from the Crystal website.[41] The screened-Coulomb HSE06 (ref. 42 and 43) range-separated hybrid functional was used to obtain accurate band gaps of the computed structures. The diagonalization of the Fock matrix was performed at adequate *k*-point grids in the reciprocal space. The thresholds controlling the accuracy of the Coulomb and exchange integrals calculations were set to 10^{-8} and 10^{-14}, and the mixing percent of the Fock/Kohn–Sham matrices was set to 40% (IPMIX keyword).[39] The band structure and the density of states (DOS) projected on the atoms and orbitals of bulk γ-Ag_2WO_4 were constructed along the appropriate high-symmetry directions of the

corresponding irreducible Brillouin zone. To confirm the character of local minima on the potential energy of the surfaces, vibrational frequency calculations were carried out to ensure that only positive frequencies corresponded to minima for the studied ordered and disordered structural models.

The disordered models were generated by creating Ag or W atom dislocations from their initial coordinates in the ordered and most stable structure. The following displacements were explored: (i) 0.05 to 0.20 Å in the *z*-coordinate of the Ag atom; (ii) 0.05 to 0.20 Å in the *z*-coordinate of the W atom; and (iii) 0.05 to 0.20 Å in the *z*-coordinate of the Ag and W atoms. These displacements were considered for 25% and 50% of all Ag or W atoms.

Stoichiometric slabs for the (100), (110) and (111) surfaces of the cubic γ-Ag_2WO_4 structure were modeled, and the surface energy value, E_{surf}, which is defined as the energy per unit area required to form the surface relative to the bulk, was calculated as follows:

$$E_{surf} = \frac{E_{slab} - nE_{bulk}}{2A} \quad (1)$$

where E_{slab} is the total energy of the 2D slab, nE_{bulk} is the energy of the corresponding amount of bulk Ag_2WO_4 units, and A represents the surface area, which is created on each side of the 2D slab and is repeated periodically. After the corresponding thickness optimization process and convergence tests, slab models consisting of four molecular units were obtained for the (100) and (111) surfaces, while six molecular units were used for the (110) surface. In addition, different slab terminations have been taken into account in order to find the E_{surf} values.

The equilibrium shape of a crystal can be calculated using the classic Wulff construction, which minimizes the total surface free energy at a fixed volume, and provides a simple relationship between the E_{surf} of the (*hkl*) plane and its distance in the normal direction from the center of the crystallite. This strategy can be used to correlate the theoretical and experimental morphologies for α and β phases of Ag_2WO_4 system.[44,45]

3. Results and discussion

3.1 XRD

The X-ray diffraction pattern of the Ag_2WO_4 sample is shown in Fig. 1. From the analysis of the peak positions and their relative intensities, we confirmed that the as-synthetized samples, with a lattice parameter of a = 9.335 Å, were consistent with the standard powder diffraction pattern of γ-Ag_2WO_4 (JCPDS file no. 861157). This lattice parameter value is in agreement with those of other isomorphous spinel compounds such as Na_2WO_4 with a = 9.13 Å,[32] Ag_2MoO_4 with a = 9.26 Å (ref. 46) and a = 9.25 Å,[47] Na_2MoO_4 with a = 9.108 Å,[48] and Ag_2WO_4 with a = 9.35 Å.[27] To confirm the γ-Ag_2WO_4 structure, the d_{hkl} and the respective relative intensity for the associate peak were compared with other reported data from similar structures as shown in Table S1 of the (ESI†).

The theoretical calculations of γ-Ag_2WO_4 yielded a lattice parameter of 9.3045 Å, which is in agreement with the experimental value obtained, and a simple fully cubic symmetry. The

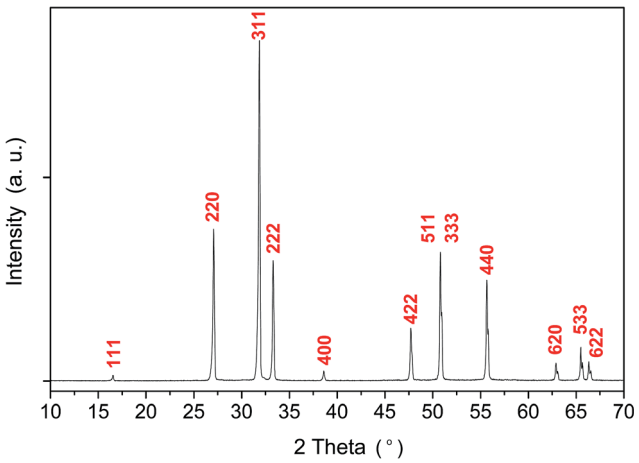

Fig. 1 XRD pattern of γ-Ag_2WO_4 with its respective Miller index.

conventional cell for this spinel structure contains 8 formula units where the W atoms occupy the tetrahedral 8a sites, the Ag atoms reside at the octahedral 16d position, and the O atoms stay at the 32e positions in the $Fd\bar{3}m$ space group, as depicted in Fig. 2. As reported by our group for α- and β-phases, the [AgO_y] and [WO_z] clusters are the common building blocks in the polyhedral representation of each unit cell.[9,15,34,45] However, difference between y and z subscripts are revealed for each structure.

3.2 FE-SEM

Different magnification FE-SEM micrographs of samples with synthesis times of 10 and 20 min are shown in Fig. 3, where the morphological evolution of the γ-Ag_2WO_4 particles can be seen. The images display a broad grain size distribution, at around 2–4 μm, and nearly spherical shapes. For the reaction time of 10 min, some small nanocrystals with a cuboid structure are visible on the large microcrystal surfaces that have not diffused into the interior. The samples corresponding to 20 min reaction time had the most microparticles with irregular or approximately spherical structures, although some faceted particles can be observed. Furthermore, a decrease in the number of

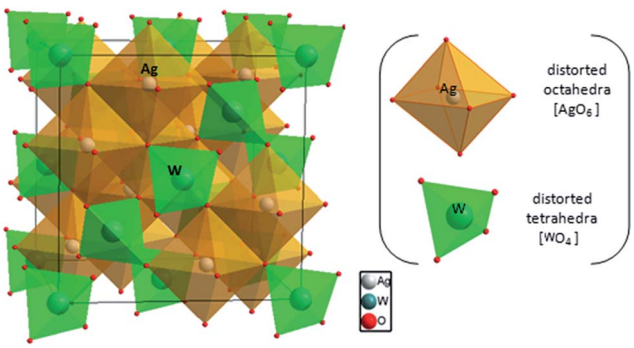

Fig. 2 A polyhedral representation of the γ-Ag_2WO_4 unit cell. Depicted are the local coordination of the Ag and W atoms corresponding to the octahedral [AgO_6] and tetrahedral [WO_4] clusters, respectively.

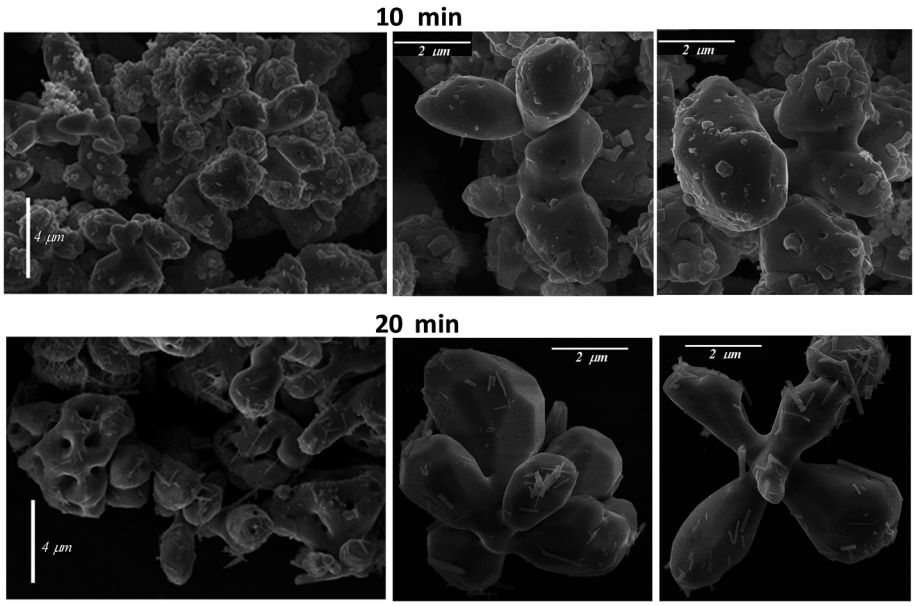

Fig. 3 FE-SEM micrographs at different magnifications for the different times of synthesis.

nanoparticles on the surface can be perceived. These nanoparticles are observed to be rod-shaped. Although our group had previously reported this rod-like morphology in the α-Ag_2WO_4 phase,[9,12,15] traces of this phase were not detected for the experimental techniques used in this work. For both reaction times, the presence of nanoparticles on the surface of the microparticles can be explained by the incomplete diffusion of these small particles into the larger γ-Ag_2WO_4 particles. This behavior suggests that an Ostwald-ripening mechanism takes place, where, when the growth kinetics are fast, bigger crystals grow at the expense of smaller nanocrystals.

To shed light on the morphology of the γ-Ag_2WO_4 phase, a theoretical analysis was performed. According to the theoretical calculations, the order of stability of the γ-Ag_2WO_4 surfaces is (110) < (100) < (111). Slab models with thickness of 9.1 Å, 9.6 Å and 9.3 Å were constructed for the (100), (110) and

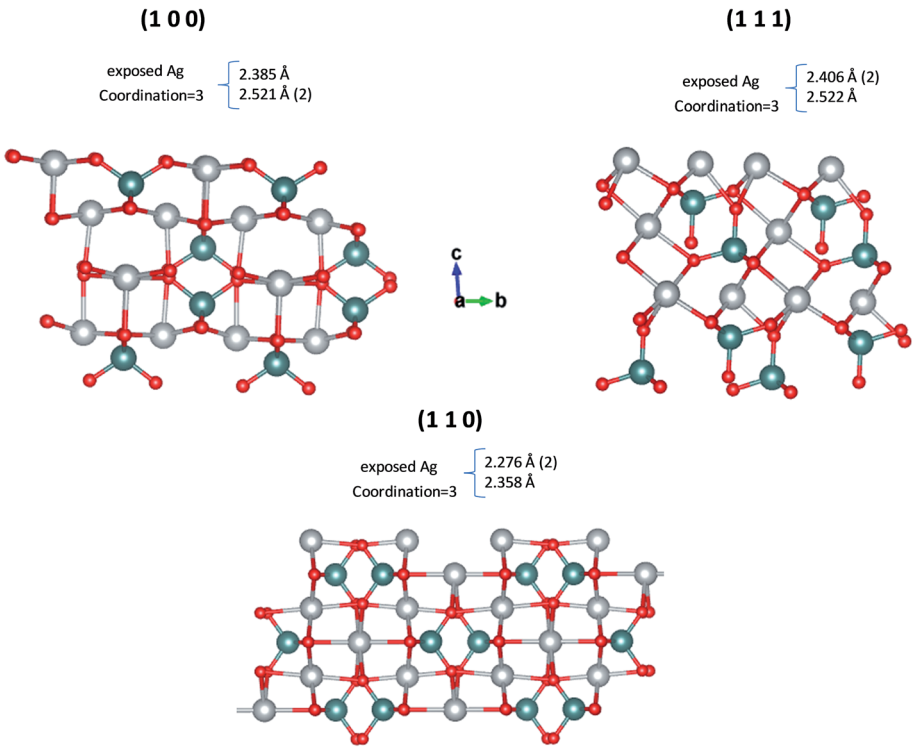

Fig. 4 Slab models constructed for (a) (100), (b) (110) and (c) (111) surfaces.

(111) surfaces, respectively. These surfaces are depicted in Fig. 4, where the most exposed Ag atoms in all surfaces are three-coordinated. The most exposed W atoms form $[WO_4]$ clusters as in the bulk. Other non-symmetric slab models constructed for the (100), (110) and (111) surfaces are presented in Fig. S1 of ESI,† which present lower stability.

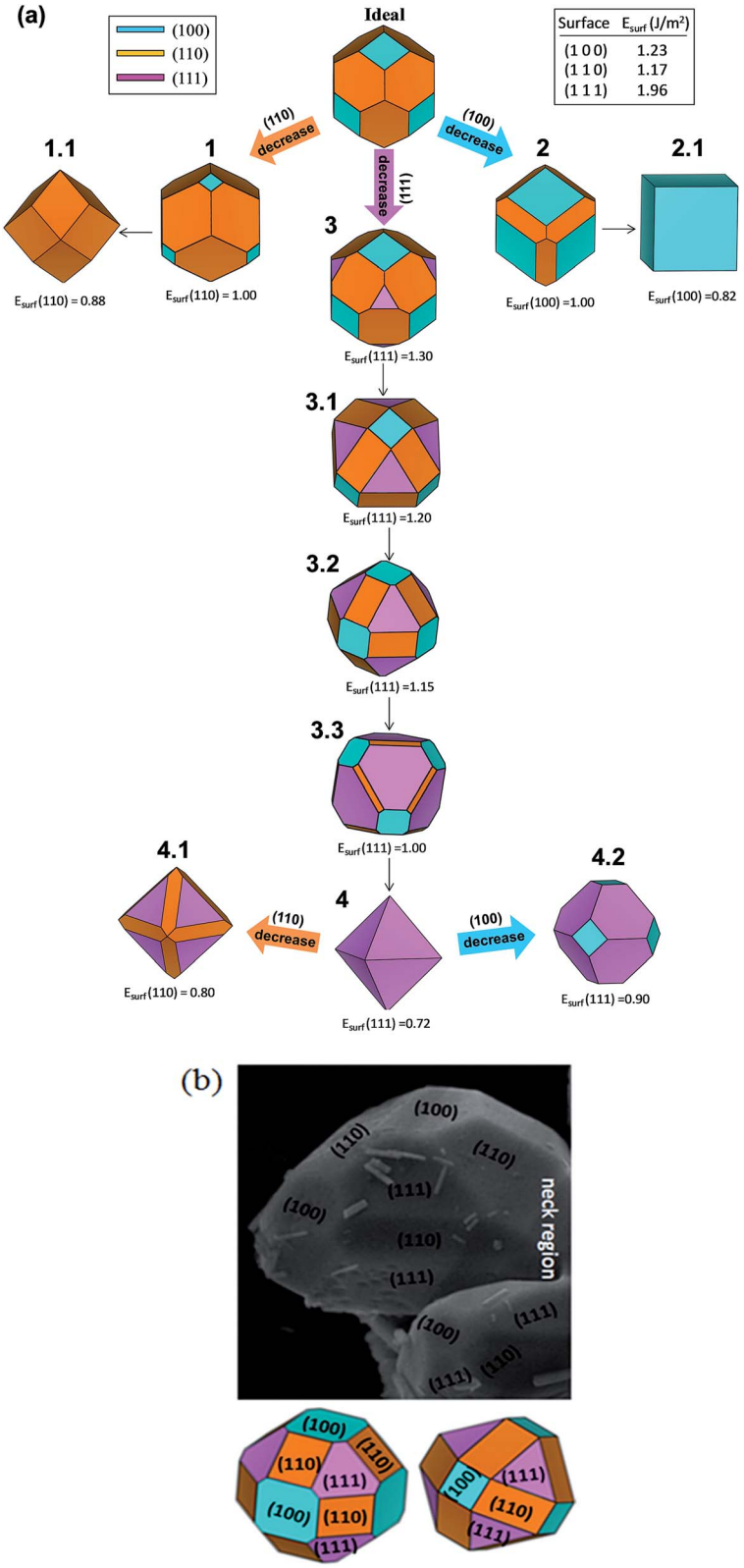

Fig. 5 (a) Theoretical morphology map for γ-Ag_2WO_4 crystals (the surface energy units are given in J m^{-2}) and (b) experimental FE-SEM images of faceted γ-Ag_2WO_4 microcrystals. The computationally simulated crystal shapes are included for comparison purposes.

From the Wulff construction, it is derived that the surfaces with the lowest surface energies control the crystal morphology.[49] The ideal morphology of γ-Ag_2WO_4 is a cube dominated by the surface (100). However, it is possible to modify this ideal morphology by tuning the surface energies of the different facets using the Wulff construction.[49–51] An analysis of the theoretical results showed that when the relative stability of the facets changes (increases or decreases), more than one type of facet will appear in the resulting morphology. We followed a model recently developed by our research group,[44,45] based on the Wulff construction, which can be used to explicitly predict the evolution of morphologies in different environments. The map of the crystal morphologies is displayed in Fig. 5a. The analysis of the theoretical results indicates that the most stable surface is the (110) followed by the (100), which form the ideal morphology (shown in the upper part of Fig. 5a). When the relative stability of the (110) and (100) facets decreased, more than one type of facet appeared in the resulting morphology. A rhombic dodecahedron (picture 1.1 of Fig. 5a) was obtained from the ideal morphology passing through picture 1, as the surface energy of the (110) facet decreased to 0.88 J m^{-2}; while a cube was produced when the surface energy of the (100) facet decreased to 0.82 J m^{-2} (see morphology 2.1). When the surface energy of the (111) facet decreased to 1.30 J m^{-2}, morphology 3 was obtained, and a subsequent decrease in the surface energy value for the (111) facet rendered the 3.1, 3.2 and 3.3 morphologies (see Fig. 5a). Finally, an octahedron was achieved when the surface energy of the (111) facet decreased to 0.72 J m^{-2} (morphology 4). The experimental FE-SEM image displayed in Fig. 5b was the best well-faceted sighting to use for comparison. A good agreement between the experimental and theoretical morphologies was obtained when the surface energy values of the (111) facet was 1.20 or 1.15 J m^{-2}. These surface energy values generated 3.1 or 3.2 morphologies, respectively. In the neck region: the particle diverted from the suggested theoretical morphology due to the neck formed with other particles. Thus, variations in the ratio between surface energy values affect the related morphologies, and can be used to obtain correlations with the experimental results. We have reported well-faceted rod-like elongated particles as typical morphology for α- and β-Ag_2WO_4 microcrystals. For these two polymorphs, a narrow range of values, between 0.2–1.4 J m^{-2} and 0.08–1.16 J m^{-2}, for α-[52] and β-,[45] respectively, were calculated for the surface energy values. In comparison, the present work displays: (i) bigger values, 1.17–1.96 J m^{-2}; and (ii) not-faceted shape for γ-Ag_2WO_4. A possible relationship between value and range of surface energy with the metastability is under review for future works.

3.3 Differential scanning calorimetry

The γ-Ag_2WO_4 thermograms are shown in Fig. 6. The DSC curve clearly shows three processes. At lower temperatures, the exothermic peak at 184 °C is linked to the γ-α phase transition. Two endothermic peaks at higher temperatures can be observed, abroad peak at 500 °C and a sharp peak at 603 °C, which can be associated to the probable decomposition of the Ag_2WO_4 and a melting process, respectively. Only the last process is reversible.

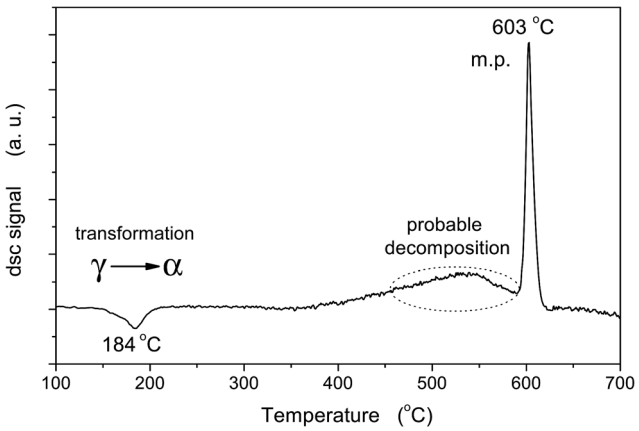

Fig. 6 DSC curves of γ-Ag_2WO_4.

3.4 Raman spectra

Raman spectroscopy is one of the most suitable methods for investigating and characterizing the structure and symmetry of solids, particularly the degree of short-range structural order, and it also provides the degree of structural order–disorder in bonds between atoms in the materials.[53] Fig. 7a shows the

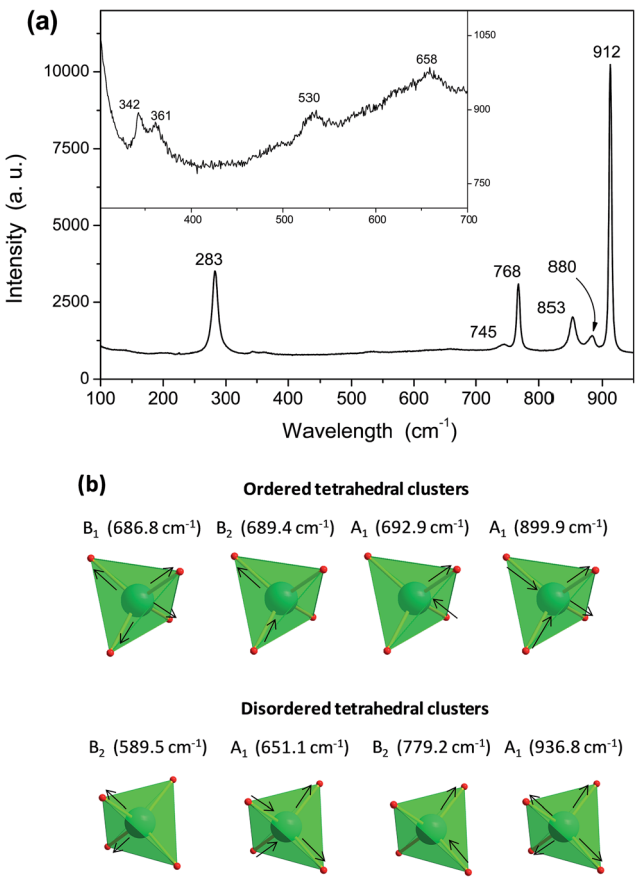

Fig. 7 (a) The micro-Raman spectra of γ-Ag_2WO_4, the inset shows the wavelength range at a lower intensity band. (b) Theoretical stretching modes in the 580–940 cm^{-1} range related to the structural rearrangement provoked by the displacement of 50% of the W atoms.

Raman spectra of γ-Ag_2WO_4 crystals, where 10 active modes are observed. An analysis of the results rendered the presence of an intense absorption band at 912 cm^{-1}, which did not appear in the other Ag_2WO_4 phases, as well as active modes at around 880 and 853 cm^{-1}. These bands, as well as others with lower intensities at 658 and 530 cm^{-1}, can be assigned to the W–O stretching bonds, and are usually present in any tungstate sample. Torsional motions of the [WO_4] clusters appeared at 361 and 342 cm^{-1}.

In order to better understand the structural arrangement and vibrational behavior of the γ-Ag_2WO_4 crystals, computational calculations were carried out. The theoretical active Raman modes (Table S2 of the ESI†) can be organized into two groups. For the ordered structure, the first group goes to 380 cm^{-1} and is composed of the internal vibrations of the symmetric and asymmetric bending of the tetrahedral [WO_4] clusters. In the second group, at higher frequencies, there are only two modes, which correspond to the asymmetric and symmetric stretching of the [WO_4] clusters at ~672 cm^{-1} and ~905 cm^{-1}, respectively.

Another interesting aspect observed in the Raman spectra is the significant increase of the bandwidth modes, which suggests that some disorder was present due to the weakening of some interatomic interactions. Disorder is used here in its most general sense, namely, any perturbations that disrupt the ideal or ordered crystal. At the time, the emphasis was on the description of the disordered crystal and these disorders were considered to be perturbations. The experimentally observed absorption peaks in the 750–850 cm^{-1} range, depending on the structural distortion related to a displacement of Ag or W atoms, can be assigned to modes obtained by theoretical calculations. This kind of behavior was also associated with a tighter arrangement of ions in the unit cell. Therefore, it is important to mention that γ-Ag_2WO_4 is formed by two groups of distorted polyhedral (octahedral [AgO_6] and tetrahedral [WO_4] clusters). Hence, we assume that tungstate groups are partially disordered, giving rise to the large bandwidth increase observed.

From all displacements explored, we have considered those that agree well with the experimental results, such as the displacement of 50% of the 0.10 Å W atoms in the *z*-coordinate, as listed in Table S2.† The displacement of 50% of the W atoms generated the higher mode at 936.8 cm^{-1} corresponding to the symmetric stretching of only the distorted clusters (half of the [WO_4] clusters), while the mode at 899.9 cm^{-1} refers to the symmetric stretching of the ordered clusters. As previously mentioned, the modes that appeared at 779.2 cm^{-1}, 651.1 cm^{-1} and 589.5 cm^{-1} are related to the asymmetric stretching of the distorted [WO_4] clusters, while the modes in the range 686–693 cm^{-1} are associated to the asymmetric stretching of the ordered clusters. Stretching modes in the range 580–940 cm^{-1} are depicted in Fig. 7b. It is worth noting that the stretching motion of the [WO_4] clusters is not affected by the displacement of any percentage of Ag atoms, and therefore it is not appropriate to explain the observed experimental modes in the 750–850 cm^{-1} range. The relative positions of the theoretical and experimental Raman-active modes are displayed in Fig. 8, where it can be observed that there is good agreement between the experimental and calculated. However, the calculated frequencies are slightly overestimated (except for both bending of disordered

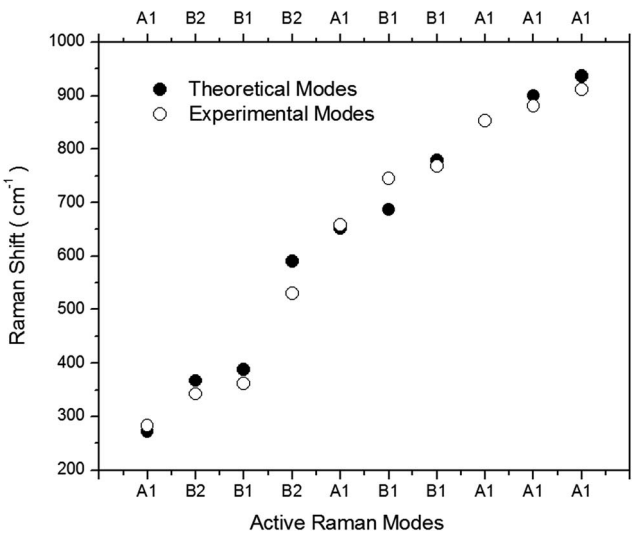

Fig. 8 Comparison between the relative positions of the theoretical and experimental Raman-active modes.

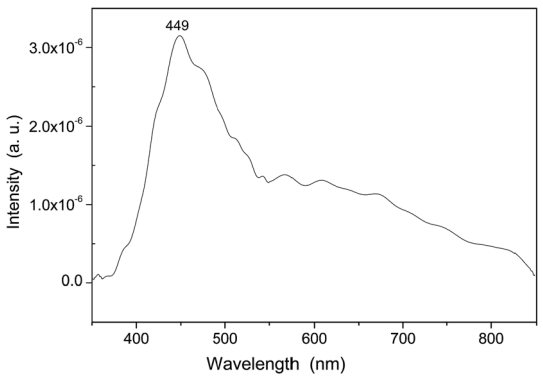

Fig. 9 PL spectra of γ-Ag_2WO_4 microcrystals.

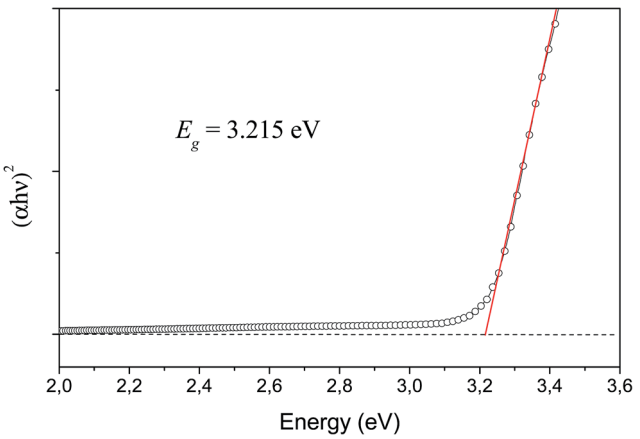

Fig. 10 UV-vis spectra of γ-Ag_2WO_4 metastable.

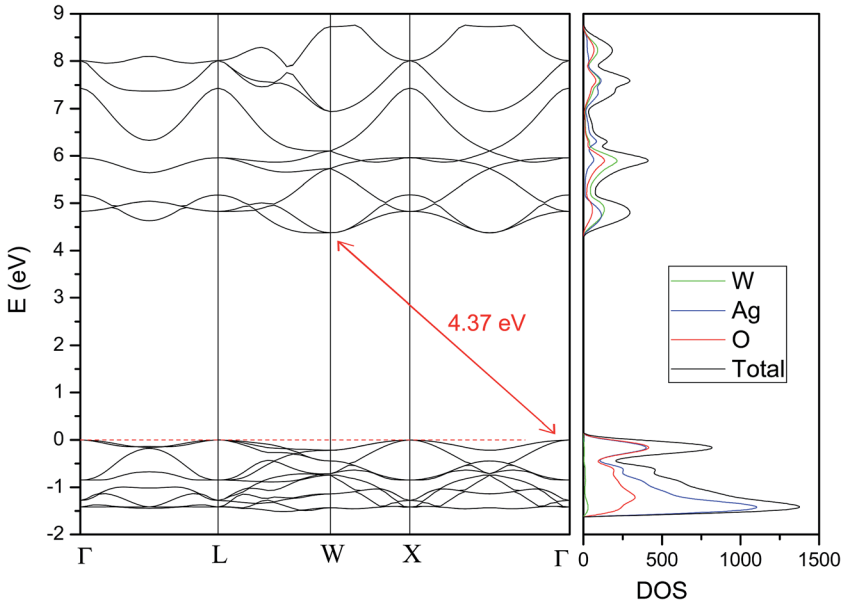

Fig. 11 Band structure and DOS projected on γ-Ag_2WO_4 atoms.

structure, A_1 mode, and stretching of both ordered, F_{2g} mode, and disordered structures, B_1, B_2 and A_1 modes) compared to experimental data. Hence, we assume that: (i) tungstate groups are partially disordered, giving rise to the large bandwidth increase in the Raman spectra, and (ii) these disordered tungstate groups are present in larger quantities than the disordered silver groups.

3.5 PL spectra

PL emission spectra are dependent on the electronic structure of the material at hand, and they are a powerful probe for structural short and medium range order–disorder effects, such as clusters in the lattice. In Fig. 9, a prominent PL emission band is clearly seen with a maximum emission at 449 nm. This emission peak in the blue region is typically related to distorted [WO_6] octahedral in the α- and β-Ag_2WO_4 crystals.[9,15,35,45] However, in our samples, it can be related to distorted [WO_4] tetrahedral. For the α-Ag_2WO_4 phase, another diffused emission in the red region, from 620 to 640 nm, can be attributed to the [AgO_y] clusters.[9,15] In our samples, any red peak obtained was an indication that the [AgO_6] clusters were less prone to be distorted. This result is in agreement with the Raman spectroscopy results.

3.6 UV spectra

The determination of the optical band gap was obtained by combining Tauc's equation[54] with the method proposed by Kubelka and Munk-Aussig,[55] which is based on the transformation of diffuse-reflectance measurements, see ESI.† Tauc's equation is the following,

$$\alpha h\nu = A(h\nu - E_{gap})^n \quad (2)$$

where E_{gap} is the optical energy gap, α is the optical absorption coefficient, $h\nu$ is the photon energy, A is a constant, and n is a constant associated with different kinds of electronic transitions ($n = 0.5$ for a direct allowed and $n = 2$ for an indirect allowed). The band gap energy was estimated from the modified Kubelka–Munk equation, see ESI.† Fig. 10 shows the UV-visible diffuse reflectance spectra for γ-Ag_2WO_4. According to literature, the optical absorption spectrum in the silver tungstate family exhibits direct electronic transitions between the valence and conduction bands;[9,13,56] therefore, in this work a $n = 0.5$ value was used in eqn (2). The band gap energy, estimated from the intercept of the tangent to the plot, was 3.21 eV.

For the theoretical band gap, we report an indirect band gap value of 4.37 eV from Γ to W (see Fig. 11), which serves as a guide to understand band gap trends, but does not directly correspond to the physically measured quantity. The difference between the experimental and theoretical band gap values can be associated to the short and medium-range distortions on the [AgO_6] and [WO_4] clusters. An analysis of the DOS projected on the atoms renders that the conduction band (CB) is mainly attributed to W atoms, while the valence band (VB) is mainly formed by O and Ag atoms. An analysis of the DOS projected on the orbitals shows that the top of the VB is formed by the hybridization of Ag 4d and O 2p orbitals, while the bottom of the CB is mainly formed by the hybridization of W 5d and O 2p orbitals.

The value of this difference, 1.16 eV, is bigger than the difference between experimental and theoretical values reported by our group for α- and β-, ~0.40 and 0.40 eV, respectively.[15,45,52] This agree with the suggestion that γ-Ag_2WO_4 is the polymorph more susceptible to be disordered.

4. Conclusions

The behavior of metastable phases is of substantial scientific and technological interest. The polymorphism of Ag_2WO_4 is

a puzzling and important problem. In this work, metastable γ-Ag_2WO_4 crystals were prepared by the precipitation method, and an in-depth physicochemical characterization of these structures was successfully performed. The theoretical models and results, along with our experimental data, allowed us to analyze the structural, morphological, vibrational, and optical properties of the γ-Ag_2WO_4 phase.

Ordered and disordered models to describe the crystal structure are considered. Disordered [WO_4] tetrahedral clusters were key to reproduce the linewidth of the bands appearing in the Raman spectra, while a prominent PL emission band with maximum emission in the blue region was related to these distorted [WO_4] tetrahedra. In addition, it was found that γ-Ag_2WO_4 has an indirect band gap, and the calculated positions of the valence and conduction bands showed the presence of [WO_4] tetrahedral and [AgO_6] octahedral clusters. These distortions can facilitate the separation and migration of electron and hole pairs, they can improve the photocatalytic performance of γ-Ag_2WO_4, and they could be the source of the metastable character of this phase. The experimental morphologies of the as-synthesized samples are similar to the theoretically obtained shapes when the surface energy values for the (111) surface was decreased.

Finally, we point out how the combination of experimental techniques with theory is the first step to better understand the chemistry of the less-common γ-Ag_2WO_4 polymorph. Therefore, this study illustrates the potential of this joint strategy, which helps to open a promising path toward fundamental information regarding the geometry, cluster coordination, and electronic structure of γ-Ag_2WO_4 crystals. The availability of a facile method to prepare γ-Ag_2WO_4 is expected to catalyze further empirical studies on the elusive and little-studied γ-phase because of its varied potential applications.

Acknowledgements

This work was financially supported by the following Brazilian research funding institutions: Fundação de Amparo à Pesquisa do Estado de São Paulo (FAPESP; 2012/14004-5 and 2013/07296-2), Conselho Nacional de Desenvolvimento Científico e Tecnológico (CNPq; 479644/2012-8, 350711/2012-7, 304531/2013-8 and 151136/2013-0). Coordenação de Aperfeiçoamento de Pessoal de Nível Superior (CAPES). J. A. acknowledges also the financial support of the Spanish research funding projects: PrometeoII/2014/022 and ACOMP/2014/270 and ACOMP72015/1202 projects (Generalitat-Valenciana), Ministerio de Economia y Competitividad (CTQ2015-652017-P) and Programa de Cooperación Científica con Iberoamerica (Brasil) of Ministerio de Educación (PHBP14-00020). J. A. acknowledges to Ministerio de Economia y Competitividad, "Salvador Madariaga" program, PRX15/00261. L. G. acknowledges Banco Santander (Becas Iberoamérica: Jóvenes profesores e investigadores). We also acknowledge the Servei Informática, Universitat Jaume I for a generous allotment of computer time.

References

1 C. C. Chen, A. B. Herhold, C. S. Johnson and A. P. Alivisatos, Size dependence of structural metastability in semiconductor nanocrystals, *Science*, 1997, **276**, 398–401.
2 M. Jansen, I. V. Pentin and J. C. Schoen, A Universal Representation of the States of Chemical Matter Including Metastable Configurations in Phase Diagrams, *Angew. Chem., Int. Ed.*, 2012, **51**, 132–135.
3 S. Shukla, S. Seal, R. Vij, S. Bandyopadhyay and Z. Rahman, Effect of nanocrystallite morphology on the metastable tetragonal phase stabilization in zirconia, *Nano Lett.*, 2002, **2**, 989–993.
4 U. Schubert and N. Hüsing, *Synthesis of Inorganic Materials*, Wiley-VCH Weinheim, 2012.
5 C. G. Levi, Metastability and microstructure evolution in the synthesis of inorganics from precursors, *Acta Mater.*, 1998, **46**, 787–800.
6 J. F. Liu, Q. H. Li, T. H. Wang, D. P. Yu and Y. D. Li, Metastable vanadium dioxide nanobelts: Hydrothermal synthesis, electrical transport, and magnetic properties, *Angew. Chem., Int. Ed.*, 2004, **43**, 5048–5052.
7 J. Lu, P. F. Qi, Y. Y. Peng, Z. Y. Meng, Z. P. Yang, W. C. Yu and Y. T. Qian, Metastable MnS crystallites through solvothermal synthesis, *Chem. Mater.*, 2001, **13**, 2169–2172.
8 J. Andrés, L. Gracia, P. Gonzalez-Navarrete, V. M. Longo, W. Avansi Jr, D. P. Volanti, M. M. Ferrer, P. S. Lemos, F. A. L. Porta, A. C. Hernandes and E. Longo, Structural and electronic analysis of the atomic scale nucleation of Ag on α-Ag_2WO_4 induced by electron irradiation, *Sci. Rep.*, 2014, **5**, 5391.
9 L. S. Cavalcante, M. A. P. Almeida, W. Avansi, R. L. Tranquilin, E. Longo, N. C. Batista, V. R. Mastelaro and M. S. Li, Cluster Coordination and Photoluminescence Properties of α-Ag_2WO_4 Microcrystals, *Inorg. Chem.*, 2012, **51**, 10675–10687.
10 X. J. Cui, S. H. Yu, L. L. Li, L. Biao, H. B. Li, M. S. Mo and X. M. Liu, Selective synthesis and characterization of single-crystal silver molybdate/tungstate nanowires by a hydrothermal process, *Chem.–Eur. J.*, 2004, **10**, 218–223.
11 Z. Lin, J. Li, Z. Zheng, J. Yan, P. Liu, C. Wang and G. Yang, Electronic Reconstruction of α-Ag_2WO_4 Nanorods for Visible-Light Photocatalysis, *ACS Nano*, 2015, **9**, 7256–7265.
12 E. Longo, L. S. Cavalcante, D. P. Volanti, A. F. Gouveia, V. M. Longo, J. A. Varela, M. O. Orlandi and J. Andres, Direct *in situ* observation of the electron-driven synthesis of Ag filaments on α-Ag_2WO_4 crystals, *Sci. Rep.*, 2013, **3**, 1676.
13 L. S. Cavalcante, V. M. Longo, J. C. Sczancoski, M. A. P. Almeida, A. A. Batista, J. A. Varela, M. O. Orlandi, E. Longo and M. S. Li, Electronic structure, growth mechanism and photoluminescence of $CaWO_4$ crystals, *CrystEngComm*, 2012, **14**, 853–868.
14 C.-X. Guo, B. Yu, J.-N. Xie and L.-N. He, Silver tungstate: a single-component bifunctional catalyst for carboxylation of terminal alkynes with CO_2 in ambient conditions, *Green Chem.*, 2015, **17**, 474–479.

15 E. Longo, D. P. Volanti, V. M. Longo, L. Gracia, I. C. Nogueira, M. A. P. Almeida, A. N. Pinheiro, M. M. Ferrer, L. S. Cavalcante and J. Andres, Toward an Understanding of the Growth of Ag Filaments on α-Ag_2WO_4 and Their Photoluminescent Properties: A Combined Experimental and Theoretical Study, *J. Phys. Chem. C*, 2014, **118**, 1229–1239.

16 E. Longo, W. Avansi Jr, J. Bettini, J. Andres and L. Gracia, *In situ* Transmission Electron Microscopy observation of Ag nanocrystal evolution by surfactant free electron-driven synthesis, *Sci. Rep.*, 2016, **6**, 21498.

17 J. W. Tang and J. H. Ye, Correlation of crystal structures and electronic structures and photocatalytic properties of the W-containing oxides, *J. Mater. Chem.*, 2005, **15**(39), 4246–4251.

18 M. Vafaeezadeh and M. M. Hashemi, One pot oxidative cleavage of cyclohexene to adipic acid using silver tungstate nano-rods in a Bronsted acidic ionic liquid, *RSC Adv.*, 2015, **5**, 31298–31302.

19 J. T.-W. Wang, J. M. Ball, E. M. Barea, A. Abate, J. A. Alexander-Webber, J. Huang, M. Saliba, I. Mora-Sero, J. Bisquert, H. J. Snaith and R. J. Nicholas, Low-Temperature Processed Electron Collection Layers of Graphene/TiO_2 Nanocomposites in Thin Film Perovskite Solar Cells, *Nano Lett.*, 2013, **14**, 724–730.

20 R. Zhang, H. Cui, X. Yang, H. Tang, H. Liu and Y. Li, Facile hydrothermal synthesis and photocatalytic activity of rod-like nanosized silver tungstate, *Micro Nano Lett.*, 2012, **7**, 1285–1288.

21 X. Sang, P. Wang, L. Ai, Y. Li and J. Bu, Preparation of fine Ag_2WO_4 antibacterial powders and its application in the sanitary ceramics, *Adv. Mater. Res.*, 2011, **284–286**, 1321–1325.

22 L. F. da Silva, A. C. Catto, W. Avansi Jr, L. S. Cavalcante, J. Andres, K. Aguir, V. R. Mastelaro and E. Longo, A novel ozone gas sensor based on one-dimensional (1D) α-Ag_2WO_4 nanostructures, *Nanoscale*, 2014, **6**, 4058–4062.

23 V. M. Longo, C. C. De Foggi, M. M. Ferrer, A. F. Gouveia, R. S. Andre, W. Avansi, C. E. Vergani, A. L. Machado, J. Andres, L. S. Cavalcante, A. C. Hernandes and E. Longo, Potentiated Electron Transference in α-Ag_2WO_4 Microcrystals with Ag Nanofilaments as Microbial Agent, *J. Phys. Chem. A*, 2014, **118**, 5769–5778.

24 W. d. S. Pereira, J. Andres, L. Gracia, M. A. San-Miguel, E. Z. da Silva, E. Longo and V. M. Longo, Elucidating the real-time Ag nanoparticle growth on α-Ag_2WO_4 during electron beam irradiation: experimental evidence and theoretical insights, *Phys. Chem. Chem. Phys.*, 2015, **17**, 5352–5359.

25 D. Xu, B. Cheng, J. Zhang, W. Wang, J. Yu and W. Ho, Photocatalytic activity of Ag_2MO_4 (M = Cr, Mo, W) photocatalysts, *J. Mater. Chem. A*, 2015, **3**, 20153–20166.

26 X.-Y. Zhang, J.-D. Wang, J.-K. Liu, X.-H. Yang and Y. Lu, Construction of silver tungstate multilevel sphere clusters by controlling the energy distribution on the crystal surface, *CrystEngComm*, 2015, **17**, 1129–1138.

27 A. J. van den Berg and C. A. H. Juffermans, The polymorphism of silver tungstate Ag_2WO_4, *J. Appl. Crystallogr.*, 1982, **15**, 114–116.

28 X. Wang, C. Fu, P. Wang, H. Yu and J. Yu, Hierarchically porous metastable beta-Ag_2WO_4 hollow nanospheres: controlled synthesis and high photocatalytic activity, *Nanotechnology*, 2013, **24**, 165602–165609.

29 J. Li, C. Yu, C. Zheng, A. Etogo, Y. Xie, Y. Zhong and Y. Hu, Facile formation of Ag_2WO_4/AgX (X = Cl, Br, I) hybrid nanorods with enhanced visible-light-driven photoelectrochemical properties, *Mater. Res. Bull.*, 2015, **61**, 315–320.

30 H. Chen and Y. Xu, Photoactivity and stability of Ag_2WO_4 for organic degradation in aqueous suspensions, *Appl. Surf. Sci.*, 2014, **319**, 319–323.

31 Y. V. B. De Santana, J. E. C. Gomes, L. Matos, G. H. Cruvinel, A. Perrin, C. Perrin, J. Andres, J. A. Varela and E. Longo, Silver Molybdate and Silver Tungstate Nanocomposites with Enhanced Photoluminescence, *Nanomater. Nanotechnol.*, 2014, **4**, 1–10.

32 P. H. Bottelberghs, E. Everts and G. H. J. Broers, Phase-Diagram and High Ionic-Conductivity of System Na_2WO_4–Ag_2WO_4, *Mater. Res. Bull.*, 1976, **11**, 263–268.

33 T. Takahashi, S. Ikeda and O. Yamamoto, Solid-State Ionics – New High Ionic Conductivity Solid Electrolyte $Ag_6I_4WO_4$ and Use of This Compound in a Solid-Electrolyte Cell, *J. Electrochem. Soc.*, 1973, **120**, 647–651.

34 R. A. Roca, P. S. Lemos, J. Andrés and E. Longo, Formation of Ag nanoparticles on metastable β-Ag_2WO_4 microcrystals induced by electron irradiation, *Chem. Phys. Lett.*, 2016, **644**, 68–72.

35 P. S. Lemos, A. Altomare, A. F. Gouveia, I. C. Nogueira, L. Gracia, R. Llusar, J. Andrés, E. Longo and L. S. Cavalcante, Synthesis and characterization of metastable β-Ag_2WO_4: an experimental and theoretical approach, *Dalton Trans.*, 2016, **45**, 1185–1191.

36 S. K. Gupta, K. Sudarshan, P. S. Ghosh, S. Mukherjee and R. M. Kadam, Doping Induced Room Temperature Stabilization of Metastable β-Ag_2WO_4 and Origin of Visible Emission in α and β-Ag_2WO_4: Low Temperature Photoluminescence Studies, *J. Phys. Chem. C*, 2016, **120**, 7265–7276.

37 G. S. Silva, M. T. Fabbro, L. Gracia, L. P. S. d. Santos, J. Andrés, E. Condorcillo, H. Beltrán-Mir and E. Longo, Theoretical and Experimental Insight on Ag_2CrO_4 Microcrystals: Synthesis, Characterization and Photoluminescence Properties, *Inorg. Chem.*, 2016, **55**, 8961–8970.

38 R. C. d. Oliveira, L. Gracia, M. Assis, M. S. Li, J. Andrés, E. Longo and L. S. Cavalcante, Disclosing the electronic structure and optical properties of $Ag_4V_2O_7$ crystals: Experimental and theoretical Insights, *CrystEngComm*, 2016, **18**, 6303–6326.

39 R. Dovesi, V. R. Saunders, C. Roetti, R. Orlando, C. M. Zicovich-Wilson, F. Pascale, B. Civalleri, K. Doll, N. M. Harrison, I. J. Bush, P. D'Arco, M. Llunel, M. Causà

and Y. Noël, *CRYSTAL14 User's Manual*, Theoretical Chemistry Group: University of Turin, Italy, 2014.

40 F. Cora, A. Patel, N. M. Harrison, R. Dovesi and C. R. A. Catlow, An *ab initio* Hartree–Fock study of the cubic and tetragonal phases of bulk tungsten trioxide, *J. Am. Chem. Soc.*, 1996, **118**, 12174–12182.

41 Crystal, http://www.crystal.unito.it/basis-sets.php.

42 J. Heyd, G. E. Scuseria and M. Ernzerhof, Hybrid functionals based on a screened Coulomb potential, *J. Chem. Phys.*, 2003, **118**, 8207–8215.

43 A. V. Krukau, O. A. Vydrov, A. F. Izmaylov and G. E. Scuseria, Influence of the exchange screening parameter on the performance of screened hybrid functionals, *J. Chem. Phys.*, 2006, **125**, 224106.

44 J. Andrés, L. Gracia, A. F. Gouveia, M. M. Ferrer and E. Longo, Effects of surface stability on the morphological transformation of metals and metal oxides as investigated by first-principles calculations, *Nanotechnology*, 2015, **26**, 405703–405713.

45 R. A. Roca, A. F. Gouveia, P. S. Lemos, L. Gracia, J. Andrés and E. Longo, Formation of Ag Nanoparticles on β-Ag_2WO_4 through Electron Beam Irradiation: A Synergetic Computational and Experimental Study, *Inorg. Chem.*, 2016, **55**, 8661–8671.

46 J. Donohue and W. Shand, The Determination of the Interatomic Distances in Silver Molybdate, Ag_2MoO_4, *J. Am. Chem. Soc.*, 1947, **69**, 222–223.

47 L. Cheng, Q. Shao, M. Shao, X. Wei and Z. Wu, Photoswitches of One-Dimensional Ag_2MO_4 (M = Cr, Mo, and W), *J. Phys. Chem. C*, 2009, **113**, 1764–1768.

48 K. G. Bramnik and H. Ehrenberg, Study of the Na_2O–MoO_3 system. $Na_6Mo_{11}O_{36}$ – a new oxide with anatase-related structure, and the crystal structures of Na_2MoO_4, *Z. Anorg. Allg. Chem.*, 2004, **630**, 1336–1341.

49 G. Wulff, On the question of speed of growth and dissolution of crystal surfaces, *Z. Kristallogr.*, 1901, **34**, 449–530.

50 J. W. Gibbs, On the equilibrium of heterogeneous substances, *Trans. Conn. Acad. Arts Sci.*, 1878, **3**, 343–524.

51 C. Herring, Some Theorems on the Free Energies of Crystal Surfaces, *Phys. Rev.*, 1951, **82**, 87–93.

52 R. A. Roca, J. C. Sczancoski, I. C. Nogueira, M. T. Fabbro, H. C. Alves, L. Gracia, L. P. S. Santos, C. P. de Sousa, J. Andrés, G. E. Luz Jr, E. Longo and L. S. Cavalcante, Facet-dependent photocatalytic and antibacterial properties of α-Ag_2WO_4 crystals: combining experimental data and theoretical insights, *Catal. Sci. Technol.*, 2015, **5**, 4091–4105.

53 J. R. Ferraro, K. Nakamoto and C. W. Brown., *Introductory Raman Spectroscopy*, Academic Press, Amsterdam, 2nd edn, 2003.

54 J. Tauc, Optical Properties and Electronic Structure of Amorphous, *Mater. Res. Bull.*, 1968, **3**, 37–46.

55 P. Kubelka and F. Munk, Ein Beitrag Zur Optik Der Farbanstriche, *Z. Med. Phys.*, 1931, **12**, 593–601.

56 D. Y. Kim, S. H. Im and O. O. Park, Synthesis of Tetrahexahedral Gold Nanocrystals with High-Index Facets, *Cryst. Growth Des.*, 2010, **10**, 3321–3323.

